CFD simulation on centrifugal pump impeller with splitter blades

Henrique M. P. Rosa[1] & Bruno S. Emerick[2]

[1] Universidade Federal de Viçosa/Departamento de Engenharia de Produção e Mecânica/Curso de Engenharia Mecânica. Viçosa, MG, Brasil. E-mail: henrique.rosa@ufv.br (Corresponding author) - ORCID: 0000-0002-1437-2265
[2] Universidade Federal de Santa Catarina/Departamento de Engenharia Mecânica/Laboratório de Engenharia de Processos de Conversão e Tecnologia de Energia. Florianópolis, SC, Brasil. E-mail: brunosemerick@lepten.ufsc.br - ORCID: 0000-0003-0118-3577

ABSTRACT: The present paper aims to present the analysis and comparison of results of computational simulations using Computational Fluids Dynamics (CFD) in impellers of centrifugal pump. Three impellers were simulated: 1) original impeller, 2) original impeller with splitter blades at outlet; 3) original impeller with splitter blades at inlet. The splitters occupied 30% of the length of the main blades. They were simulated using the ANSYS-CFX software system in 1500 rpm rotational speed and at different flow rates. The turbulence model assumed was the Shear Stress Transport (SST). The results were used to build impeller blade head curves, besides the presentation of pressure distribution and streamline behaviour inside the impeller. It was verified that the insertion of the splitter blades reduced the impeller blade head, mainly the impeller with outlet splitter, whose reduction was more intense.

Key words: turbomachinery design, flow modeling, pressure distribution, streamline behavior

Simulação CFD em rotor de bomba centrifuga com pás intermediárias

RESUMO: A proposta deste artigo é apresentar a análise e comparação dos resultados de simulação computacional usando a Dinâmica dos Fluidos Computacional (CFD) em rotores de bomba centrífuga. Três rotores foram simulados: 1) rotor original; 2) rotor original com pás intermediárias na saída; 3) rotor original com pás intermediárias na entrada. O comprimento das pás intermediárias foi de 30% do comprimento da pá principal. Eles foram simulados usando o software ANSYS-CFX na rotação de 1500 rpm para diferentes vazões. O modelo de turbulência adotado foi o Shear Stress Transport (SST). Com os resultados foram construídas as curvas de altura produzida pelas pás do rotor, além da apresentação da distribuição de pressão e comportamento das linhas de corrente dentro do rotor. Foi verificado que a inserção das pás intermediárias levou à redução da altura produzida pelas pás do rotor, principalmente para o rotor com pás intermediárias na saída, na qual a redução foi maior.

Palavras-chave: projeto de turbomáquinas, modelagem de escoamento, distribuição de pressão, comportamento de linhas de corrente

Introduction

The computational fluid dynamics (CFD) is the present day state-of-art technique in fluid flow analysis (Choi et al., 2013). Successful results in predicting the flow patterns within the passages of centrifugal pumps indicate that CFD might be capable of assisting a pump engineer in obtaining improved designs (Yedidiah, 2008). Several researchers have studied pump optimization using the CFD tool.

Chakraborty et al. (2012) studied the effect of the number of impeller blades on the performance of centrifugal pumps. For the pump studied, ten blades presented better results.

Yang et al. (2012) used CFD technology to explore the reasons for performance variation on pump as turbine (PAT) when the impeller diameter is trimmed.

Wang et al. (2017) studied a special impeller used on pump as turbine (PAT). In that study, hydraulic loss, internal flow characteristic, and static pressure distribution were analyzed on the basis of the two PATs' numerical results obtained by CFD.

Zhu et al. (2016) investigated the utilization of half vane diffuser in a centrifugal pump with 6- blade impeller. For the half vane diffusers, the same vanes were used, except for the vane height.

Nataraj & Singh (2014) discuss the response surface methodology (RSM)-based design optimization of a centrifugal pump complemented with CFD simulations.

In this context, this study aims to apply a CFD simulation software system to study the behaviour of a radial impeller of a centrifugal pump, with splitter blades inserted between the main blades. A comparison will be carried out with the original impeller (without splitter blades).

Material and Methods

The original impeller had six blades and its design operating flow rate was 52 m³ h⁻¹ at 1500 rpm rotation speed. Table 1 lists the main geometric design parameters of this impeller. The Figures 1A and B show the original impeller.

The three impellers simulated were: 1-original impeller; 2-original impeller with insertion of splitter blades at outlet; 3-original impeller with insertion of splitter blades at inlet. These impellers were named, respectively: impeller#1, impeller#2 and impeller#3. The splitter blade length was 30% of the main blade length. Figure 1C shows the section view of impeller#2, which is similar to the impeller #3, except that the splitters are at the inlet.

In the averaging of the steady-state incompressible flows, the conservation equations can be solved based on the average

Table 1. Main geometric parameters of the impeller

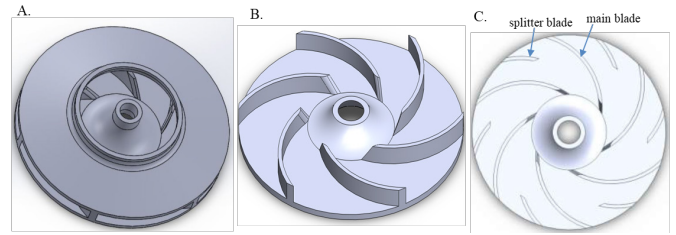| Daxis	D4	D5	Bt	b5	β4	β5	z
			(mm)			(°)	
20	110	235	4.0	15.3	39.0	28.22	6
Daxis	Axis diameter						
Bt	Blade thickness						
D4	Inlet diameter						
D5	Outlet diameter						
b5	Outlet width						
β4	Inlet blade angle						
β5	Outlet blade angle						
z	Number of blades						

Figure 1. Isometric view of impeller (A), section view of impeller (B), and section view of impeller with outlet splitter blades (C)

Reynolds values or the time-averaging approach. However, the most common method for modeling turbulent flows is the time-averaging method. Using this approach for the case of incompressible flows, the general forms of the governing equations are as described by Eqs. 1 to 5. Since a rotating control volume is considered, these equations employ the relative motion and, therefore, the relative velocity of fluid - W (Jafarzadech et al., 2011).

Since the pumped fluid is incompressible and the flow is in a steady state, the continuity equation is composed as follows:

$$\vec{\nabla}\vec{W} = 0 \qquad (1)$$

where:

W   - relative velocity of fluid.

Besides, the equation of conservation of momentum is expressed as relation (Eq. 2). This is the three dimensions Navier-Stokes equation for rotary domain.

$$\rho\left(\vec{W}\vec{\nabla}\right)\vec{W} = -\vec{\nabla}P + \vec{\nabla}\tau + S_M \qquad (2)$$

where:

ρ   - fluid density;
P   - static pressure;
τ   - shear stress tensor, related to fluid viscosity; and,
S_M - source term, related to additional forces.

For flows in a rotating frame of reference at a constant angular velocity ω, additional sources of momentum are required to account for the effects of the Coriolis force and the centrifugal force (Jafarzadech et al., 2011), written as Eqs. 3 and 4, respectively:

$$S_{Cor} = -\rho\vec{\omega}x\vec{W} \qquad (3)$$

$$S_{Cfg} = -\rho\vec{\omega}x\left(\vec{\omega}x\vec{r}\right) \qquad (4)$$

where:

S_{cor} - Coriolis force;
S_{cfg} - centrifugal force;
ω   - angular velocity; and,
r   - location vector.

Thus, the additional sources of momentum is written as Eq. 5:

$$S_M = -\rho\vec{\omega}x\vec{W} - \rho\vec{\omega}x\left(\vec{\omega}x\vec{r}\right) \qquad (5)$$

The CFD finite volume method is the most used to solve problems. This method models three-dimensional flow. Since the method is a fully-implicit solver, it creates no time step limitation and is considered easy to implement. It is also a coupled solver, which means that the momentum and continuity equations are solved simultaneously. This approach reduces the number of iterations required to obtain convergence and no pressure correction term is required to retain mass conversion. Therefore, it is a more robust and accurate solver (Barrio et al., 2010; Derakhshan et al., 2012).

Prior knowledge about the phenomenon analyzed and the application of the boundary conditions or the flow parameters are necessary to ensure the reliability of the results.

In this context, a high-quality mesh must be generated. The numerical mesh is the discretization of the fluid domain, where the variables for the flow simulation will be calculated. In 3D simulation in the impeller, the width of flow channel varies along the radius.

After the generation of the fluid domain for each impeller configuration, the mesh is generated by the system called Meshing in ANSYS Workbench.

For meshing, regardless the impeller configuration, the CFD model was adopted in Physics Preference and the CFX was selected as the Solver Preference. The CFX Solver presents very accurate results and can afford to run a fine mesh. Refinements in the mesh were made near the edges on the fluid domain, which is a region of interest for the occurrence of physical phenomena.

The User Advanced Size Function is used for growth control and mesh distribution in key areas with high curvature or near the surface. The Sizing function was set up as On Curvature, which imposes a growth rate for the transition between the sizes of cell, ensuring a smaller normal curvature angle, thereby creating a finer mesh surface. In Max Face Size and Max Size, the values established were 0.002 m. Both functions determine the max size related to the elements in the mesh.

Figure 2 shows the mesh of the fluid domain for the impeller with six splitter blades at the outlet. It is a non-structured

Figure 2. Mesh generated with six splitter blades at outlet (impeller#2)

tetrahedral mesh, which resulted in 301271 nodes after a meshing independence test.

Regarding the boundary conditions, this project focus on the fluid domain generated from the impeller. The boundary conditions set up were: static pressure (101325 Pa) at inlet and mass flow rate at outlet. The variation of outlet mass flow allowed to simulate design and several off-design operation conditions.

The remaining parts were set as the Wall, which is a boundary impenetrable to the flow. The wall was set as No Slip, and the roughness of the wall was set as 100 microns, due to the manufacturing process.

The turbulence model applied was the Shear Stress Transport (SST). This model is very accurate for the numerical investigation of flow within a centrifugal pump (Shojaeerd et al., 2012), also used by other authors, including Akemi et al. (2015) and Li et al. (2018)

The fluid domain is a rotary domain with constant rotational speed of 1500 rpm. Therefore, all boundary rotated with this speed, except the inlet, which was stationary.

The fluid was defined as water at 25 °C.

The disk friction losses and the flow leakage were not considered in the simulations. Consequently, the hydraulic head produced represents the specific work transmitted by the impeller blades. This is calculated by Eq. 6:

$$H_{blade} = \frac{\Delta P}{\rho g} \qquad (6)$$

where:

H_{blade} - Impeller blade head, in m;

ΔP - Total pressure difference (static + dynamic) between the Inlet and Outlet, in Pa;

ρ - Density of the water, in kg m^{-3}; and,

g - Gravity acceleration, in m s^{-2}.

Where water density is 997 kg m^{-3} (at 25 °C), and gravitational acceleration as 9.80665 m s^{-2}. The rotational speed, 1500 rpm, was maintained for all simulations.

RESULTS AND DISCUSSION

The impeller blade head curve was built for each impeller simulated, as shown in Figure 3.

Figure 3 shows that the insertion of splitter blades reduced the impeller blade head. This may be due to: 1) the increased friction on the impeller, since, when the splitter blades are inserted, the fluid flows in contact with a larger solid rough surface inside the impeller; 2) change in the direction of the relative flow.

The latter can reduce the angle of relative flow by leaving impeller β_2, which results in $\beta_{2'} < \beta_2$ so that β_2 is the blade angle at the outlet (Figure 4A). According to Euler equation (Eq. 7), which is based on ideal conditions, the maximum specific work transferred by the impeller is obtained when $\beta_{2'} = \beta_2$, since the tangential component of absolute velocity V_{t2} is the maximum. When $\beta_{2'} < \beta_2$, the tangential component of absolute velocity at outlet $V_{t2'}$ is smaller than V_{t2} (Figure 4B). Consequently, the
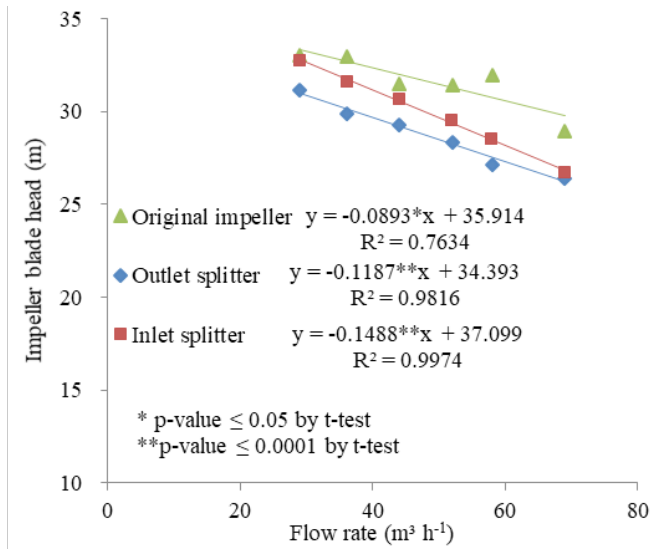
Figure 3. Impeller blade head as a function of flow rate for three impellers

specific work transmitted by the impeller decreases (Pfleiderer & Petermann, 1979; Stepanoff, 1957; Turton, 1995).

$$H_{blade} = \frac{u_2 V_{t2} - u_1 V_{t1}}{g} \qquad (7)$$

where:

　　u_1　　- tangential velocity at inlet;
　　u_2　　- tangential velocity at outlet;
　　V_{t1}　　- tangential component of absolute velocity at inlet; and,
　　V_{t2}　　- tangential component of absolute velocity at outlet.

　　Figure 5 shows the total pressure distribution and the stream lines in a middle plane inside the impeller for 52 m³ h⁻¹ flow rate (nominal rate) for the three impellers simulated.

　　The pressure distributions (Figures 5A, C and E) show similarity between the impellers and compatibility with the turbomachinery theory: the pressure energy increases along the radius of the impeller.
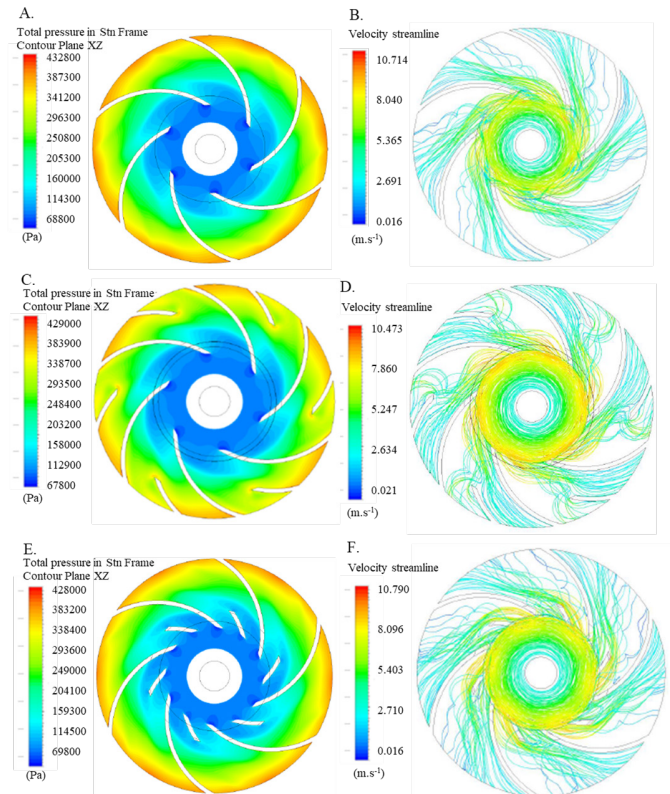

Figure 5. Pressure distributions on: Original impeller (A), impeller with splitter at outlet (C), impeller with splitter blade at the inlet (E); stream line distribution on: Original impeller (B), impeller with splitter at the outlet (D), impeller with splitter blade at the inlet (F)

　　The pressure distribution on the outlet region of impeller#2 (Figure 5C) is less uniform, compared to the other two. There is greater pressure between the back-face of the splitter blade and the front-face of the main blade. No similar phenomenon is observed on the inlet region in impeller#3 (Figure 5E). In other words, the pressure on the inlet region in impeller#3 is more uniform than on the outlet region in impeller#2. This indicates that the splitter blades at the outlet cause more disturbance on pressure distribution than the splitter blade at the inlet.
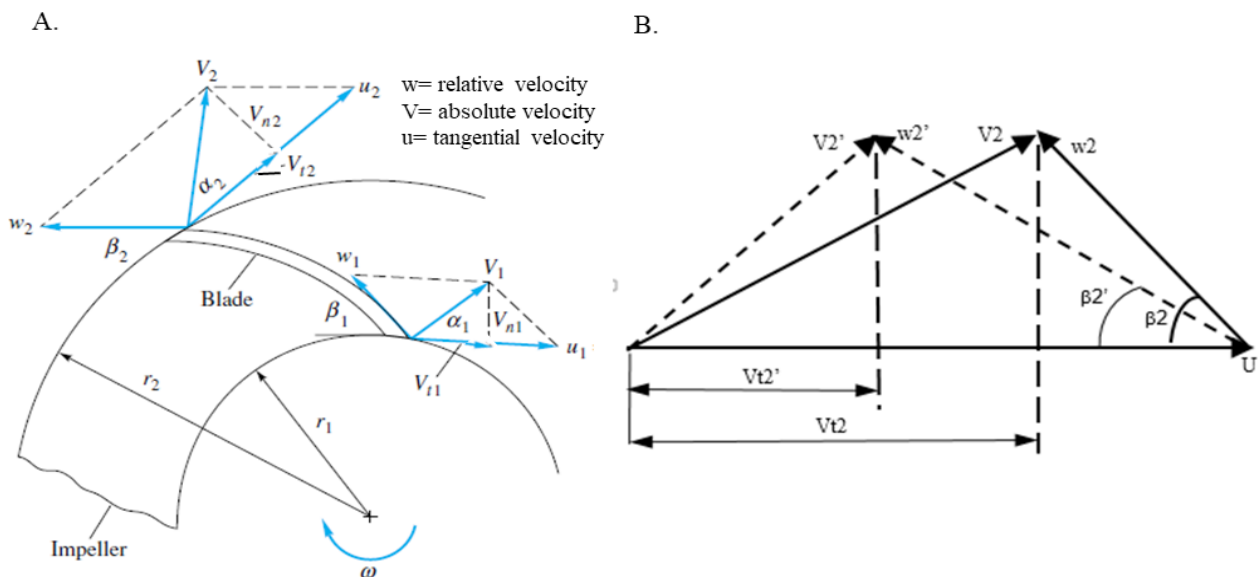

Figure 4. Ideal inlet and outlet velocity diagram (A), ideal and real velocity diagram at the outlet (B)

The streamlines show the path that a small, neutrally-buoyant particle would take through the flow domain (Ansys, 2011). It was set up to show 250 lines for the simulations (Figures 5B, D and F).

Within the original impeller, the concentration of flow is larger on the front-face of the blade (Figure 5B), due to the Coriollis force action over the relative flow (Sedille, 1967).

According to Stepanoff (1957), a great quantity of blades provides better guided and more uniform flow inside the impeller, which can increase the hydraulic energy produced by the impeller. However, a great number of blades increases energy loss due the viscous friction. Therefore, a splitter blade is inserted in order to make the flow more uniform and better guided, which increases the impeller blade head, without increasing much the friction loss.

Figures 5D and F show that the splitter deviated part of the fluid stream. In the impeller with outlet splitter, the deviation did not occur smoothly. Instead, there was a hard curvature on the stream (Figure 5D), which caused energy loss. For the impeller with inlet splitter, the curvature on the streamline at the downstream splitter was smooth. The deviation on the stream line modified the pressure distribution, in agreement with the turbomachinery theory, according to which there is a relation between pressure and the velocity approached by the Bernoulli equation (Sedille, 1967).

Conclusions

1. The insertion of the splitters reduced the impeller blade head when compared to the impeller without splitters. Thus, the outlet splitter caused greater reduction.

2. The splitter caused some deviations on the flow and energy loss, mainly the outlet splitters, which caused a hard curvature on the stream.

3. The splitter at the inlet improved flow distribution, despite the smooth flow curvature at the downstream edge of the splitter. Additionally, the viscous friction raised with the splitters, which reduced the impeller blade head.

4. The CFD simulation led to results that agree with the turbomachinery theory.

5. The CFD approach may help improving the existing efficiency measuring techniques and the evaluation of the performance pumps, besides the development of new impeller design.

Acknowlegdment

Literature Cited

Akemi, H.; Nourbakhsh, S. A.; Raisee, M.; Najafi, A. F. Development of new multivolute casing geometries for radial force reduction in centrifugal pumps. Engineering Applications of Computational Fluid Mechanics, v.9, p.1-11, 2015. https://doi.org/10.1080/19942060.2015.1004787

Ansy Inc. Ansys CFD-Post user's guide. United States: SAS IP Inc., 2011. 356p.

Barrio, R.; Parrondo, J.; Blanco, E. Numerical analysis of the unsteady flow in the near-tongue region in a volute-type centrifugal pump for different operating points. Computers & Fluids, v.39, p.859-870, 2010. https://doi.org/10.1016/j.compfluid.2010.01.001

Chakraborty, S.; Pandey, K. M.; Roy, B. Numercial analysis on effects of blade number variations on perfomance of centriugal pumps with various rotational speeds. International Journal of Current Engineering and Technology, v.2, p.143-152, 2012.

Choi, H.-J.; Zullah, M. A.; Roh, H.-W.; Ha, P.-S.; Oh, S.-Y; Lee, Y.-H. CFD validation of perfomance improvement of a 500kW Francis turbine. Renewable Energy, v.54, p.111-123, 2013. http://dx.doi.org/10.1016/j.renene.2012.08.049

Derakhshan, S.; Yang, S.-S.; Kong, F.-Y. Theoritical, numerical and experimental prediction of pump as turbine performance. Renewable Energy, v.48, p.507-513, 2012. http://dx.doi.org/10.1016/j.renene.2012.06.002

Jafarzadech, B.; Hajari, A.; Alishahi, M. M.; Akbari, M. H. The flow simulation of a low-specific-speed high-speed centrifugal pump. Applied Mathematical Modelling, v.35, p.241-249, 2011. https://doi.org/10.1016/j.apm.2010.05.021

Li, D.; Wang, H.; Li, Z.; Nielsen, T. K.; Goyal, R.; Wei, X.; Qin, D. Transient characteristics during the closure of guide vanes in pump-turbine mode. Renewable Energy, v.118, p.973-983, 2018. https://doi.org/10.1016/j.renene.2017.10.088

Nataraj, M.; Singh, R. R. Analyzing pump impeller for perfomance evaluation using RSM and CFD. Desalination and Water Treatment, v.52, p.6822-6831, 2014. https://doi.org/10.1080/19443994.2013.818924

Pfleiderer, C.; Petermann, H. Máquinas de fluxo. Rio de Janeiro: Livros Técnicos e Científicos Editora, 1979. 454p.

Sedille, M. Turbomachines hydrauliques et thermiques. Tome 2. Paris: Masson & Cie Éditeurs, 1967. 572p.

Shojaeerd, M. H.; Tahani, M.; Ehghaghi, M. B.; Fallahian, M. A.; Beglari, M. Numerical study of the effects of some geometric characteristics of a centrifugal pump impeller that pumps a viscous fluid. Computers & Fluids, v.60, p.61-70, 2012 http://dx.doi.org/10.1016/j.compfluid.2012.02.028

Stepanoff, A. J. Centrifugal and axial flow pumps: Theory, design and applications. New York: John Wiley & Sons Inc., 1957. 462p.

Turton, R. K. Principles of turbomachinery. 2.ed. London: Chapman & Hall, 1995. 265p.

Wang, T.; Wang, C.; Kong, F.; Gou, Q.; Yang, S. Theoritical, experimental, and numerical study of special impeller used in turbine mode of centrifugal pump as turbine. Energy, v.130, p.473-485, 2017. https://doi.org/10.1016/j.energy.2017.04.156

Yang, S.-S.; Kong, F.-Y.; Jiang, W.-M.; Qu, X.-Y. Effects of impeller trimming influencing pump as turbine. Computers & Fluids, v.67, p.72-78, 2012. http://dx.doi.org/10.1016/j.compfluid.2012.07.009 .

Yedidiah, S. A study in the use of CFD in the design of centrifugal pumps. Engineering Applications of Computacional Fluid Mechanics, v.2, p.331-343, 2008. https://doi.org/10.1080/19942060.2008.11015233

Zhu, X.; Li, G.; Jiang, W.; Fu, L. Experimental and numerical investigation on application of half vane diffusers for centrifugal pump. International Communnications in Heat and Mass Transfer, v.79, p.114-127, 2016. https://doi.org/10.1016/j.icheatmasstransfer.2016.10.015